Journal of Nanoparticle Research (2006) 8: 693–703
DOI 10.1007/s11051-006-9102-9
© Springer 2006

Technology and applications

Sticking efficiency of nanoparticles in high-velocity collisions with various target materials

Philipp Reissaus[1,*], Tomas Waldemarsson[2,3], Jürgen Blum[4], Dominik Clément[5], Isabel Llamas[6], Harald Mutschke[6] and Frank Giovane[7]
[1]*Space Technologies & Applications Division, Kayser-Threde GmbH München, Wolfratshauser Str. 48, 81379, München, Germany;* [2]*Department of Astronomy, University of Florida, Gainesville, FL 32611, USA;* [3]*Department of Meteorology, Stockholm University, Svante Arrhenius väg 12, 10691, Stockholm, Sweden;* [4]*Institut für Geophysik und extraterrestrische Physik, TU Braunschweig, Mendelssohnstr. 3, D-38106, Braunschweig, Germany;* [5]*Diehl BGT Defence GmbH & Co. KG, Fischbachstrasse 16, D-90552, Roethenbach a. d. Pegnitz, Germany;* [6]*Astrophysikalisches Institut der Friedrich Schiller Universität Jena, Schillergässchen 2-3, 07745, Jena, Germany;* [7]*Naval Research Laboratory, 4555 Overlook Ave SW, Washington, DC 20375-5320, USA; *Author for correspondence (E-mail: philipp.reissaus@kayser-threde.com)*

Received 22 September 2005; accepted in revised form 22 March 2006

Key words: nanoparticles, sticking efficiency, mesospheric dust, magic dust, sounding rocket, laser ablation, laser pyrolysis, noctilucent clouds, NLC, polar mesospheric summer echoes, PMSE, meteoric smoke, TEM film, TEM grid, Al_2O_3, carbon, particle-wall interactions, aerosols

Abstract

In order to find reliable collector surfaces for the Mesospheric Aerosol – Genesis, Interaction and Composition (MAGIC) sounding rocket experiment, intended to collect atmospheric nanoparticles, the sticking efficiency of nanoparticles was measured on several targets of different materials. The nanoparticles were generated by a molecular beam apparatus in Jena, Germany, by laser ablation (Al_2O_3 particles, diameter 5–50 nm) and by laser pyrolysis (carbon particles, diameter 10–20 nm). In a vacuum environment ($> 10^{-5}$ mbar) the particles condensed from the gas phase, formed a particle beam, and were accelerated to $\sim$1 km/s. The sticking efficiency on the target materials carbon, gold and grease was measured by a microbalance. Results demonstrate moderate to high sticking probabilities. Thus, the capture and retrieval of atmospheric nanoparticles was found to be quantitatively feasible.

Introduction

About 100 tons of meteoric material enters the earth's atmosphere every day (Love & Brownlee, 1993). Most of this material evaporates in the altitude range 80–100 km, i.e. the mesosphere. Subsequent recondensation of the vaporized material is believed to form particles in the nanometer size range, also known as meteoric smoke (Hunten et al., 1980). It was proposed that meteoric smoke is involved in a number of atmospheric phenomena, e.g., providing condensation nuclei for ice particles detected as noctilucent clouds and polar mesospheric summer echoes (Thomas, 1991; Plane, 2000). Until now, however, these nanometer-sized particles neither have been sampled nor directly detected using remote sensing techniques. The particles are too small to be detected optically

and they do not carry enough momentum to produce detectable electrical pulses upon impact (e.g. Grün et al., 1992). A fraction of this mesospheric dust is believed to be charged by the surrounding plasma and recent sounding rocket experiments have detected charged dust particles (e.g. Gelinas et al., 1998; Horányi et al., 2000, Rapp et al., 2005).

An international team of scientists under the guidance of the Naval Research Laboratory in Washington DC, USA, is conducting *in-situ* sampling of this meteoric smoke in the mesosphere, using a recently developed sounding rocket instrument, MAGIC (Mesospheric Aerosol – Genesis, Interaction and Composition). The MAGIC instrument was designed to collect meteoric smoke particles as the rocket ascends through the mesosphere and – for the first time ever – bring them back for detailed laboratory analyses.

The first two sounding rocket campaigns with the MAGIC instrument have recently been completed at Esrange, Sweden, in January 2005 and at Wallops Island, USA, in May 2005. Detailed laboratory analysis of the collected samples is currently underway. The next flight for the MAGIC instrument is planned for 2006 with launch from Norway.

Goal of investigation

To assess the collection capability of the MAGIC instrument it is crucial to find and study appropriate collector surfaces and determine their sticking efficiency. Hence, pre-flight laboratory experiments with potential sampling targets and nanometer-sized particles of astrophysical relevance and impact velocity, corresponding to the maximum velocity of the sounding rocket (~1 km/s), were undertaken.

Particles and targets

Two kinds of particle materials were used: Al_2O_3 particles in an O_2 atmosphere and carbon particles in a He atmosphere. Both materials can be considered as relevant with regard to the anticipated meteoric origin of the mesospheric dust. Standard transmission electron microscopy (TEM) grids with carbon films were selected as potential targets for the envisaged sticking efficiency experiments. These TEM targets consist of a thin film, which is supported by a metallic grid. Since the TEM films are extremely thin (~nm), even carbon nanoparticles are visible on a carbon TEM film (see TEM Figures below). An inherent side-asset of this kind of target is the simple post-processing of the retrieved samples. Data on the TEM grids used in this investigation are listed in Table 1.

Experimental set-ups

Two different ways of producing nanometer-sized particles were applied: (1) Al_2O_3 particles were generated by laser ablation, and (2) carbon particles were generated by laser pyrolysis.

In the case of laser ablation a YAG (Yttrium Aluminum Garnet) laser was focused on a rotating, solid aluminum target (see Figure 1). The target was surrounded by an O_2 atmosphere acting as cooling or buffer gas. As the vaporized Al atoms collided with the O_2 molecules, they cooled down, condensed, and thus formed nanometer-sized particles (typically ~5–50 nm). It is assumed that the temperature of these particles was at approximately room temperature (T = 291 K), when the particles hit the target, as the gas was in equilibrium with the walls of the reaction chamber. Data on the laser ablation are summarized in Table 2.

Table 1. Data on TEM films & grids

Manufacturer	PLANO W. Plannet GmbH/Wetzlar, Germany	PELCO International	SPI supplies
Grid diameter (mm)	3.05	3.05	3.05
Kind of mesh	200, 300	400	200
Grid material	Copper	Copper	Copper
Name of film	S 160, S 160-3	1822	G200
Film material	Carbon	Carbon	Carbon
Thickness of film (nm)	5–10	2–3	5–10

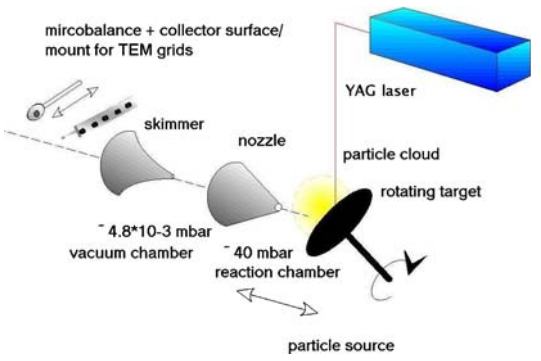

Figure 1. Sketch of laser ablation set-up.

In the case of laser pyrolysis a CO_2 laser was focused on the outlet of a double gas tube (see Figure 2). The inner tube contained the reaction gas C_2H_2 (acetylene), from which the carbon particles were generated. A photocatalytic gas (SF_6) was added to raise the energy level in the reaction gas, and eventually to produce a plasma with an average temperature of ~3000–30,000 K. The outer tube contained helium as a buffer or cooling gas. Similar to laser ablation, the molecules of the cooling gas collided with the plasma, and thus nanometer-sized particles were formed via condensation (condensation temperature ~1500 K, typical particle diameter: ~10–20 nm). In the case of carbon particles, the particle temperature is assumed to be room temperature (T = 291 K), when the particles hit the target due to the equilibrium of gas and reaction chamber walls. Data on the laser-pyrolysis setup is summarized in Table 2.

By means of a pressure gradient the generated particle cloud was in both cases directed through a nozzle from the reaction chamber into the first vacuum chamber and accelerated to supersonic speed. This way a collimated particle beam was formed. To retain a supersonic free particle jet, a skimmer was positioned in the so-called 'silent zone' of the supersonic continuum free-jet expansion (Scoles, 1988) between the first and the second vacuum chamber, in which the sampling surface/TEM film was allocated in a high vacuum environment (~10^{-4}–10^{-5} mbar) (see also Figures 1 and 2).

Experimental procedures

Two sessions of pre-flight laboratory experiments were performed, one in 2002, the other in 2003. The first session aimed to get a basic impression of the sticking efficiencies of Al_2O_3 particles and carbon particles on the selected target materials. In the second session of experiments it was decided to focus only on carbon particles due to their higher relevance (i.e. particle speed) for the envisioned MAGIC experiments and refine the laboratory experiments by means of a single chopper (a slotted plate) for velocity selection. The general

Table 2. Data on laser ablation (left column) and laser pyrolysis (middle and right column)

	First session of Al_2O_3 particle experiments (2002)	First session of carbon particle experiments (2002)	Second session of carbon particle experiments (2003)
Laser frequency (Hz)	20	20	20
Laser power (W)	2.3	0.51	7–9.1
Wavelength of laser (μm)	0.532	10.6	10.6
Laser voltage (kV)	N/A	22	N/A
Laser gas (%)	N/A	30 CO_2, 30 N_2, 40 He	10.5 CO_2, 1.5 N_2, 88 He
Laser gas flow (l/h)	N/A	60	0.5–10
Frequency of rotating target (Hz)	0.5–1.0	N/A	N/A
Nozzle diameter (mm)	0.8	0.3	0.4
Skimmer diameter (mm)	1.0	1.0	1.0
Pressure in reaction chamber (mbar)	39–44	~300–330	~300–330
Pressure in first vacuum chamber (mbar)	4.4–5.2×10^{-3}	~2.0–5.5×10^{-2}	~1.1–6.3×10^{-2}
Pressure in second vacuum chamber (mbar)	N/A	~4.0–7.5×10^{-4}	~1.3–8×10^{-5}
Gas flow (sccm)	O_2: 170	He: 500, SF_6: 30, C_2H_2: 70	He: 500, SF_6: 20, C_2H_2: 30

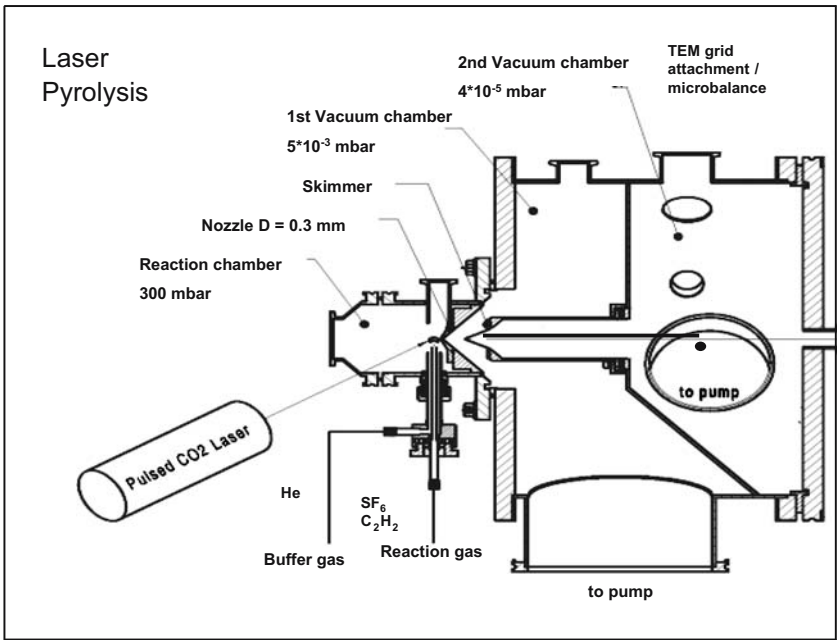

Figure 2. Sketch of laser pyrolysis set-up.

experimental procedures described hereunder hold true for both sessions.

In a first step, the particle beam was directed onto TEM targets, to get an idea of particle flux, size distribution, agglomeration status, and required experiment duration. The resulting TEM images were used to clarify, whether an appropriate experiment duration had been selected, since it was crucial to generate not more than a mono layer of particles to investigate the sticking efficiency between target and particles and not the sticking efficiency among the particles. In a second step a microbalance, either coated with a carbon film (equal to the material of the carbon TEM film) or with a reference material, intersected the particle beam, and thus measured the accumulation rate of particles, which adhered to its surface. For the microbalance measurements it was necessary to know the particle mass density, which we assume to be equivalent to that of the bulk material (Al_2O_3: 4.0 g/cm^3, C: 1.5 g/cm^3). Data on the microbalance can be found in Table 3.

All measurements were performed relative to a greased reference collector surface, with an assumed sticking efficiency close to unity. Unfortunately, it turned out to be difficult to deposit a thin layer of grease on the microbalance plates without exceeding the effective range of the microbalance (Braycote vacuum grease, properties see Table 4). Only a careful manual coating provided the necessary low thickness. To guarantee better reproducibility in terms of

Table 3. Data on quartz microbalance

Manufacturer	tectra/Frankfurt am Main, Germany
Effective range (nm)	0.1–999.9
Thickness of plate (mm)	0.2
Diameter of plate (mm)	14.0
Diameter of coated plate (mm)	6.9

Table 4. Data on Braycote vacuum grease

Manufacturer	Structure Probe, Inc./ West Chester, USA
Indication	Braycote Micronic 803 vacuum grease
Chemical Family	Fluorocarbons, fluoropolymers
Solubility in water	Insoluble
Boiling point	Decomposes >260°C
Vapor pressure (mbar)	$<\sim 1.3\times10^{-10}$
Density (g/cm^3)	<1.0

experimental target preparation, we used a second reference with a gold surface that could be handled more reliably. Standard microbalance crystals are manufactured with a gold surface coating and were therefore readily available. The first step was to establish the sticking relation between grease and gold. Once this was completed, gold was used as the reference material and compared to the sticking efficiencies of the carbon TEM films.

Particle velocities

Theoretical considerations & error analysis

During the experiments with Al_2O_3 particles, it was found that two kinds of particles were produced: spheres of about 50 nm diameter and smaller particles of about 5 nm size, with the smaller particles outnumbering the spheres by far (see Figure 3). No satisfying explanation for this bimodal size distribution has yet been found.

To estimate the particle impact velocities, it is necessary that the particles be completely coupled to the gas flow, whose velocity is known. The speed of sound of the gas in the nozzle is given by

$$v_{\text{sound}} = \sqrt{\frac{\gamma \times R \times T}{M}} \tag{1}$$

with γ being the dimensionless heat capacity ratio of the gas, $R = 8.3144$ J/(K×mol) the universal gas constant, T the temperature of the gas molecules, and M the molecular mass of the gas molecules. For an O_2 atmosphere used for the Al_2O_3 particles, $\gamma = 7/5$, $M = 32$ g/mol, and therefore, (assuming room temperature, $T = 291$ K, for the oxygen molecules) $v_{\text{sound/O2}} = 325$ m/s.

For a He atmosphere used for the carbon particles $\gamma = 5/3$, $M = 4$ g/mol, and therefore, $v_{\text{sound/He}} = 993$ m/s (assuming room temperature, $T = 291$ K, for the He molecules).

One should note that the gas reaches sound speed inside the nozzle and is further accelerated behind the nozzle (supersonic expansion). The solid particles can only reach above velocities, if they are completely coupled to the gas flow. Provided that they are perfectly coupled, the time the particles stay inside the nozzle can be estimated assuming a nozzle length of $l_{\text{nozzle}} \sim 1$ mm:

$$t_{\text{nozzle}} = \frac{l_{\text{nozzle}}}{v_{\text{sound}}}. \tag{2}$$

For an O_2 atmosphere, one gets $t_{\text{O}_2,\text{nozzle}}$, ~3 μs, for a He atmosphere $t_{\text{He,nozzle}} \sim 1$ μs.

The time τ_F the particles require to be coupled to the gas flow can be estimated in the free molecular flow regime to be

$$\tau_F = \frac{m_{\text{particle}}}{\frac{4}{3} \times \sigma_S \times \rho_{\text{gas,nozzle}} \times v_{th}}. \tag{3}$$

Here, m_{particle} is the mass of one single particle, σ_{particle} is the particle's geometric cross-sectional area, $\rho_{\text{gas,nozzle}}$ is the mass density of the gas in the nozzle, v_{th} is the mean thermal velocity of the gas molecules.

Assuming that the particles are spherical, m_{particle} is given by

$$m_{\text{particle}} = 4/3 \times r^3 \times \pi \times \rho_{\text{particle}}, \tag{4}$$

where r is the particle radius and ρ_{particle} the mass density of the particle. The cross-sectional area of one single particle is given by

$$\sigma_{\text{particle}} = r^2 \times \pi. \tag{5}$$

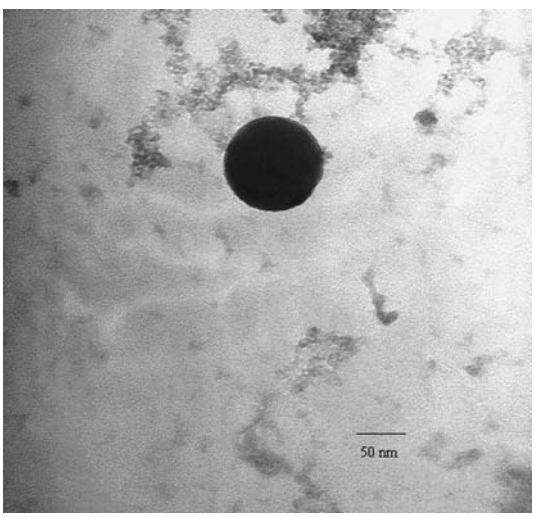

Figure 3. Two different kinds of Al_2O_3 particles on a carbon TEM film (PLANO S 160): smaller and big, spherical particles without chopper (first session of experiments (2002)).

For both kinds of gas atmospheres a certain volume flow was given (O_2: 170 sccm, He: 500 sccm, see also Table 2). For reference: 1 sccm is defined as 1 cm^3/min at standardized conditions (temperature: 0°C, pressure: 1013 mbar). One can calculate the mass flow using the density of the gas

$$\dot{m} = \rho \times \dot{V}, \tag{6}$$

with $\dot{m}$ being the mass flow and $\dot{V}$ the volume flow.

To obtain the volume flow inside the nozzle the equation of continuity is applied:

$$\dot{V}_{\mathrm{gas,nozzle}} = A \times v_{\mathrm{sound}} \tag{7}$$

with A being the cross-sectional area of the nozzle. The volume flow in the O_2 atmosphere $\dot{V}_{\mathrm{O_2,nozzle}}$ is 1.63×10^{-4} m^3/s, in the He atmosphere $\dot{V}_{\mathrm{He,nozzle}} = 7.01 \times 10^{-5}$ m^3/s. Hence, the density of the gas in the nozzle $\rho_{\mathrm{gas,nozzle}}$ can be derived:

$$\rho_{\mathrm{gas,nozzle}} = \frac{\dot{m}_{\mathrm{gas}}}{\dot{V}_{\mathrm{gas,nozzle}}}. \tag{8}$$

To verify these results, the corresponding pressures can be estimated and compared to the displayed pressures during the experiments using

$$p_{\mathrm{gas,nozzle}} = \frac{\rho_{\mathrm{gas,nozzle}}}{\rho_{gas}} \times 1\mathrm{bar}. \tag{9}$$

For laser ablation in the O_2 atmosphere $p_{\mathrm{O_2,nozzle}} = 17.4$ mbar (compared to 40 mbar displayed by the gauge), for laser pyrolysis in the He atmosphere $p_{\mathrm{He,nozzle}} = 119$ mbar (compared to 300 mbar displayed by the gauge) is calculated. Hence, these numbers are in reasonable agreement.

The mean thermal velocity of the gas molecules can be obtained by

$$v_{th} = \sqrt{\frac{8kT}{\pi m_{\mathrm{gas}}}}, \tag{10}$$

with $k = 1.3807\times10^{-23}$ J/K being Boltzmann's constant and m_{gas} the mass of a gas molecule.

Table 5. Results for τ_F

Particles	τ_F (μs)	t_{nozzle} (μs)
Al_2O_3, spherical particles (in O_2)	9.2	3
Al_2O_3, smaller particles (in O_2)	0.92	3
C (in He)	0.3	1

Assuming again room temperature (T = 291 K), $v_{\mathrm{He,th}}$ = 1241 m/s and $v_{\mathrm{O_2,th}}$ = 439 m/s are obtained.

Subsequently, τ_F can be calculated and the results are shown in Table 5. In case of spherical Al_2O_3 particles, $t_{\mathrm{nozzle}} < \tau_f$ means that the particles are not perfectly coupled to the gas flow, and their velocity can be estimated to about one third of the speed of sound of the gas flow in the nozzle (~100–200 m/s). The smaller Al_2O_3 particles, which are the vast majority among the Al_2O_3 particles, are well coupled to the gas flow according to the above calculations, and thus their velocity is ~400–500 m/s. The carbon particles also perfectly couple to the gas flow, hence their velocity is ~1000–1100 m/s, which corresponds to the maximum speed of the sounding rocket.

From the pressure verification an error analysis with regard to τ_F and, thus, the particle velocities can be done. For Al_2O_3 particles and for carbon particles the displayed pressures compared to the estimated pressures differ in both cases by a factor of ~2.5. Therefore, we assume the real pressures to be in the middle between estimated (= lower limit) and displayed pressures (= upper limit). If we apply these new pressure values for the calculation of the time τ_F the particles require to be coupled to the gas flow, τ_F will decrease (see equation (3)). This means that the particles couple even faster to the gas flow (see Table 5). Hence, the estimated values for τ_F can be regarded as maximum time values of the particles to be coupled to the gas flow. This also confirms the velocity estimations for the small Al_2O_3 and all carbon particles.

Above velocity estimations can be considered as average velocities for the majority of particles, since the unknown velocity increase by supersonic expansion is assumed to be balanced by slightly lower velocities of fractal agglomerates with fractal dimension $D \leq 2$ (see below and Figure 4) due to their slightly lower surface-to-mass ratio. We estimate the mean error with regard to the particle velocity to be ±40%.

Empirical proof

Apart from above theoretical calculations, there was also an empirical proof that pointed towards a particle velocity of the desired range for carbon particles. In former experiments, not related to this investigation, but also involving carbon particles,

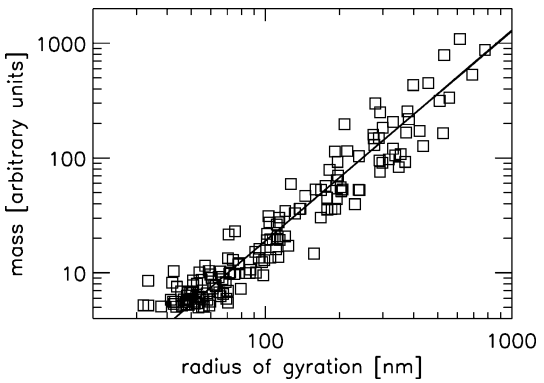

Figure 4. Determination of the fractal dimension of the carbon agglomerates. The masses of individual agglomerates with m ≤ 5 in arbitrary units (squares) are plotted as a function of their radii of gyration. The solid line is a least squares fit to the data and has a slope of $D = 1.83$.

a slotted plate, i.e. a single chopper, was installed in the experimental set-up.

The way the chopper works (see Figure 5) is that it prevents slower particles and particle agglomerates from reaching a target by reducing the time slot the particles have to move to the target to a time period immediately after the start of the particle production. Thus, only the first and fewer aggregated particles are able to pass through the chopper slot, the succeeding particles/agglomerates are blocked (the longer the particles remain inside the reaction chamber, the more time they have to agglomerate and form larger aggregates). Thus, the chopper allows only a certain particle/agglomerate velocity regime to reach the target.

The correct synchronization between rotation velocity (thus, the position of the chopper slot) and the initiation of the laser shots to start the reaction could be accomplished by assuming the carbon particle velocity and a certain delay time (between laser shot and the chopper slot position to allow particles to pass). After several experiments the particle velocity that gave the best results was 1000 m/s. This became evident by sharp-edged carbon depositions on the chopper wheel, which resulted in a heavy black film on one side of the slot that became lighter and faded towards the other side of the chopper where lower-velocity particles stuck (see Figure 5).

This means that particles having a velocity of ~1000 m/s have the highest probability to pass through the chopper slot, since the chopper slot is set to be fully open upon arrival of particles at ~1000 m/s. For particles >1000 m/s and <1000 m/s the effective slot opening is smaller and, thus, the probability of these particles to pass is reduced.

Results

In general, we did not observe counter-flow diffusion with a continuous leak of atoms and small particles into the particle beam. On the contrary, in the experiments with a chopper the microbalance did hardly detect any more particles after half a rotation of the chopper wheel.

Al_2O_3 particles without chopper (first session (2002))

As already mentioned above, two different particle sizes and forms were produced: spherical particles of ~50 nm in diameter and smaller particles of ~5 nm in diameter. It could be observed that the spherical particles were generated in the beginning of the experiments, whereas the smaller particles were produced after ~1 min, once the Al_2O_3

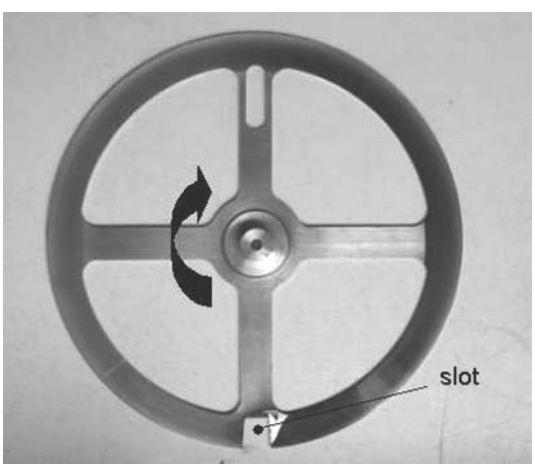

Figure 5. Empiric proof of particle velocity: on the right-hand side of the chopper slot a dense carbon film can be found, which becomes less thick along the circumference (i.e. with increasing time), when advancing counter-clockwise, indicating that the fastest particles were transmitted by the chopper (please note: the light spot on the right side next to the chopper slot originates from a finger print.)

particle generation had started. Figure 3 shows Al_2O_3 particles on a carbon TEM film after 5 min of exposure. It is evident that a mixture of single particles and agglomerates had reached the target.

Agglomeration behind the nozzle can be excluded due to supersonic expansion, in which no particle interaction is possible. Particle agglomeration on the target itself is also not a realistic possibility because

(1) if charges were responsible for the agglomeration, then all particles would be charged to an equal sign (possibly negatively, due to their origin in a plasma), which would efficiently prevent coagulation and
(2) for neutral particle agglomeration on the target, we would expect a particle-cluster agglomeration process (because the particles arrive one by one), which does not result in open structures (see Figures 3, 6, 7). Thus, we conclude that the particle agglomeration took place in front of the nozzle or during transition through the nozzle. This is also true for the carbon particle experiments.

The microbalance measurements displayed a nearly linear particle growth on all different targets. Average growth rates and derived sticking efficiencies are presented in Table 6.

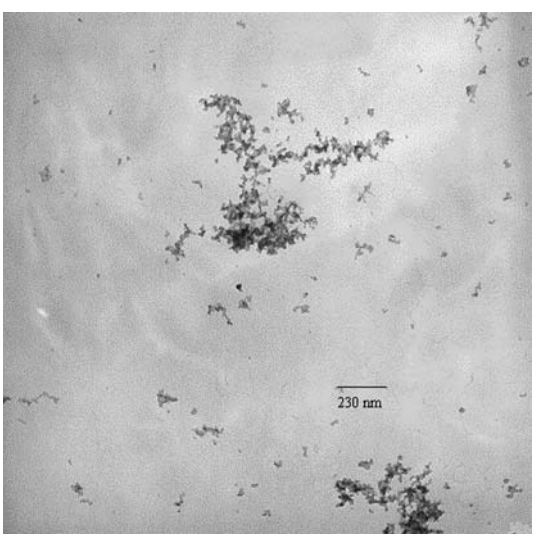

Figure 6. Carbon particles on carbon TEM film (PLANO S 160-3): single particle and fractal agglomerates without chopper (first session of experiments (2002)).

Carbon particles without chopper (first session (2002))

The first session of experiments involving carbon particles was conducted without chopper (see details above). The experiment duration was set to 30 s to exclude particle–particle sticking on the targets. A mixture of single particles and agglomerates reached the targets (see Figures 6 and 7). As for the Al_2O_3 particles, the microbalance displayed a nearly linear growth rate on any target. Average growth rates with upper and lower limits and derived sticking efficiencies for carbon particles without chopper are presented in Table 6.

Carbon particles with chopper (second session (2003))

A second session of experiments with carbon particles was carried out using the same laser pyrolysis apparatus as described above, except for two modifications. First, a new more powerful CO_2 laser had been installed (data on laser see Table 2), and second, a single chopper wheel (Figure 5) was introduced in the particle beam and mounted just in front of the collection surface with the wheel being rotated at a frequency of 20 Hz.

Also, a new technique using a special spatula facilitated the deposition of a thin uniform film of Braycote grease on the microbalance during the second session. Thus, it was easier to directly compare the sticking efficiencies of the carbon film and Braycote vacuum grease, so that gold as a second reference surface was no longer required.

As in the first session of measurements, TEM was used to characterize the carbon particles produced by the laser pyrolysis and subsequently accelerated onto the sampling surface. Despite introducing the chopper into the particle beam, with the purpose to increase the fraction of single particles, we found that the particles on the TEM grids in general showed a similar mixture of single particles and agglomerates as in the first session of experiments and partially even an increased amount of aggregates (Figure 4).

We performed a fractal analysis of the agglomerates from both experimental runs with carbon particles (sessions 1 & 2). For this, we derived a measure of the mass of each agglomerate on the available TEM images by integrating its absorption over the background in arbitrary units.

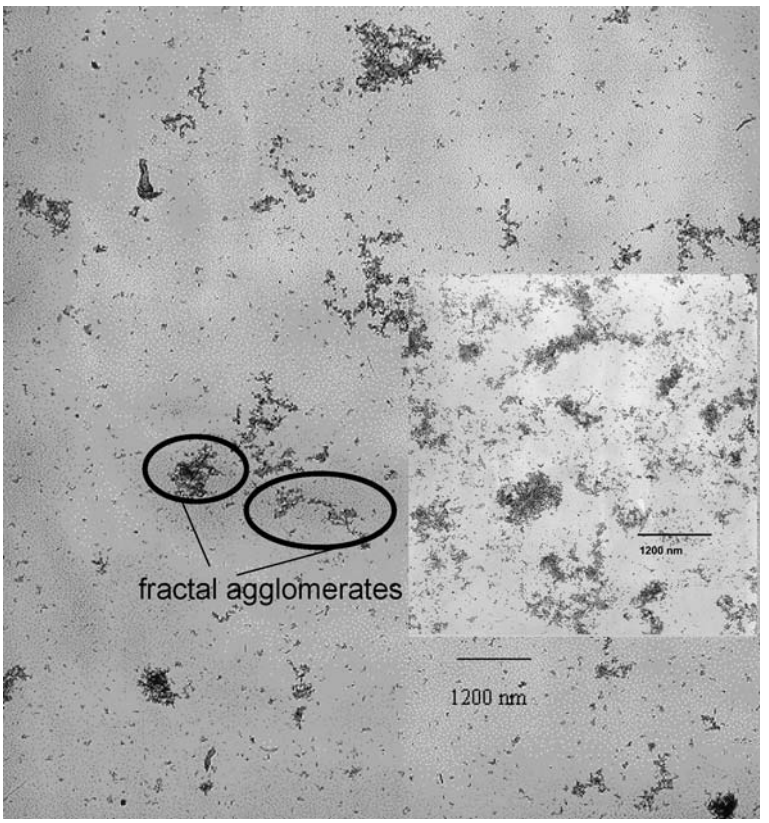

Figure 7. Comparison: carbon particle distribution after 30 s without chopper (first session of experiments (2002), large image, PLANO S 160-3) and carbon particle distribution after 30 s with chopper (second session of experiments (2003), small image, SPI G 200), indicating examples of fractal agglomerates.

Then we calculated from the projected aggregate structures the individual two-dimensional radii of gyration of the aggregates which are proportional to the three-dimensional radii of gyration. Finally, we plotted the mass m of the agglomerates as a function of their radii of gyration s in a double-

Table 6. Growth rates and sticking efficiencies of carbon and Al_2O_3 nanoparticles on various target materials (both sessions of experiments 2002 and 2003, with and without chopper)

Particle material	Chopper	Surface 1	Growth rate 1 (nm/s)	Surface 2	Growth rate 2 (nm/s)	Relative sticking efficiency surface 1/surface 2 (%)	Absolute sticking efficiency surface 1/grease (%)
Al_2O_3	No	Gold	$0.75 \pm 0.07 \times 10^{-3}$	Grease	$5.3 \pm 0.7 \times 10^{-3}$	17	17
Al_2O_3	No	Carbon	$5.3 \pm 1.9 \times 10^{-3}$	Gold	$6.3 \pm 2.3 \times 10^{-3}$	83	14
C	No	Gold	$19.8 \pm 4.0 \times 10^{-3}$	Grease	$24.3 \pm 7.9 \times 10^{-3}$	81	81
C	No	Carbon	$9.0 \pm 3.0 \times 10^{-3}$	Gold	$31.0 \pm 3.0 \times 10^{-3}$	29	24
C	Yes	Carbon	$17.9 \pm 1.8 \times 10^{-3}$	Gold	$20.6 \pm 2.1 \times 10^{-3}$	86	–
C	Yes	Carbon	$13.2 \pm 1.3 \times 10^{-3}$	Grease	$15.9 \pm 1.6 \times 10^{-3}$	83	83
C	Yes	Carbon	$11.4 \pm 1.1 \times 10^{-3}$	Grease	$15.2 \pm 1.5 \times 10^{-3}$	75	75

Please note that the given error ranges for growth rate 1 and 2 are also affected by the experimental conditions (e.g. beam conditions, particle flux, position/orientation of microbalance in beam, potential change of nozzle/skimmer diameter due to clogging). This partially results in significant ranges, which can theoretically lead to sticking efficiencies $>100\%$.

logarithmic manner (see Figure 4). The data unambiguously show that the aggregate structures are fractal, i.e. the mass-size relation follows a power law of the form

$$m \propto s^D, \tag{11}$$

where D is the so-called fractal dimension. The fractal dimensions for the carbon agglomerates range between $D = 1.60$ and $D = 1.85$. Weitz and Oliveria (1984) showed that for fractal agglomerates with $D \leq 2$ the correct fractal dimension can be obtained from projected two-dimensional images.

Table 6 lists the measured growth rates with upper and lower limits and derived sticking efficiencies. Intriguingly, all three measurements, in which a chopper was applied, indicate considerably larger sticking efficiencies compared to the first session of measurements. The growth rate being of the same order as the growth rate without the chopper also indicates that the particle production was higher with the new laser.

During the measurements with the chopper, we also investigated, whether the sticking efficiency changed as a layer of particles built up on the target surface. The results from this extended measurement (> 30 s), in which nozzle and skimmer were not clogged by adhering particles, do not indicate significant changes in the sticking efficiency, when a thicker layer of nanoparticles built up.

Discussion

From the above described experiments, we derive three major aspects about formation and sticking probabilities of nanoparticles:

(1) Al_2O_3 and carbon particles, in all kind of forms, i.e. single particles or fractal agglomerates, and in the nanometer size range, do stick after impacts at high velocities with a moderate, partially even high efficiency, to targets of carbon, gold and grease.
(2) Although a single chopper was used to separate out agglomerates, the number of fractal carbon agglomerates apparently increased in the second session of experiments. This is obviously due to an enhanced production of nanoparticles by the significantly more powerful laser beam.
(3) Despite (2) (or perhaps because of (2)?) the sticking efficiencies for carbon particles in the second session of experiments were significantly higher compared to the numbers obtained in the first session.

It is apparent that the new laser (by a factor 10 more powerful than in the previous experiments) used during the measurements with the chopper resulted in a large increase of particle production. This is confirmed by both the TEM analyses and the measured growth rates reported above. This increase of particle production is obviously the reason for the increased abundance of agglomerates.

Nevertheless we need to point out that due to the chopper the vast majority of carbon particles, which reached the target, had velocities of $\sim$1000 m/s. The chopper also prevented larger particles and/or agglomerates consisting of larger particles from reaching the sample target. This means that during the first session of experiments a wider particle size distribution, consisting of single particles (small and large) and fractal agglomerates (with small and large particles), was able to reach the target due to the absence of the chopper. Assuming that the sticking efficiency of large particles is significantly smaller than the sticking efficiency of small particles (which holds at least true in the micron region (Poppe et al., 2000)) and noting that the stricking threshold for fractal agglomerates with $D \leq 2$ is close to that of the corresponding monomer grains (Dominik & Tielens, 1997; Blum & Wurm, 2000), we can conclude that fractal agglomerates consisting of large particles stick noticeably less efficiently than fractal agglomerates with small monomers. Hence, we may obtain an explanation for the different results for the sticking efficiencies of carbon particles on carbon, gold and grease during the two sessions of experiments. Thus, in the first session of experiments a noticeable number of large particles and fractal agglomerates of large particles stuck only partially or not at all to the target, while during the second session, supported by a significantly increased number of produced particles and the particle velocity selection by the chopper, a finer particle size distribution, including fractal agglomerates of

smaller particles, was able to reach and stick to the target surface. Therefore, we can see in Figure 7 a similar structure in both TEM images: some fractal agglomerates and a significant amount of single particles.

However, due to the finer particle size distribution in the second session the number density of particles/agglomerates in the TEM image of the second session is remarkably higher. We believe that this, together with an increased particle generation, is the reason, why the sticking efficiency of carbon particles in the first session of experiments is noticeably lower than in the second session of experiments.

Conclusion

In summary, the following conclusions can be drawn from both sessions of experiments:

(1) Carbon and Al_2O_3 nanoparticles and agglomerates thereof at velocities of the order of $\sim$1 km/s have moderate to high sticking probabilities with targets of Au and C.
(2) Standard TEM grids with carbon films can be used to quantitatively capture atmospheric nanoparticles with atmospheric sounding rockets traveling at $\sim$1 km/s and retrieve them for future laboratory analyses.
(3) By this method, number density, primary particle properties, and agglomeration status of mesospheric dust can be deduced.

Acknowledgements

We would like to thank the Astrophysical Institute of the Friedrich Schiller University Jena/Germany for providing the experimental equipment and analytical instruments during the two sessions of laboratory experiments. MAGIC is a NASA project funded under grant no. NDPR S-06215-G.

References

Blum J. & G. Wurm, 2000. Experiments on sticking, restructuring, and fragmentation of pre-planetary dust aggregates. Icarus 143, 138–146.

Dominik C. & A.G.G.M. Tielens, 1997. The physics of dust coagulation and the structure of dust aggregates in space. Astrophys. J. 480, 647–673.

Gelinas L.J., K.A. Lynch, M.C. Kelley, S. Collins, S. Baker, Q. Zhou & J.S. Friedman, 1998. First observation of meteoritic charged dust in the tropical mesosphere. Geophys. Res. Lett. 25, 4047–4050.

Grün E., H. Fechtig, J. Kissel, D. Linkert, D. Maas, J.A.M. McDonnell, G.E. Morfill, G. Schwehm, H.A. Zook & R.H. Giese, 1992. The Ulysses dust experiment. Astron Astrophys Suppl Ser 92(2), 411–423.

Horányi M., S. Robertson, B. Smiley, J. Gumbel, G. Witt & Walch, 2000. Rocket-borne mesospheric measurement of heavy charge carriers. Geophys. Res. Lett. 27, 3825–3828.

Hunten D.M., R.P. Turco & O.B. Toon, 1980. Smoke and dust particles of meteoric origin in the mesosphere and thermosphere. J. Atm. Sci. 37, 1342–1357.

Love S.G. & D.E. Brownlee, 1993. A direct measurement of the terrestrial mass accretion rate of cosmic dust. Science 262, 550–553.

Plane J.M.C., 2000. The role of sodium bicarbonate in the nucleation of noctilucent clouds. Ann. Geophys. 18, 807–814.

Poppe T., J. Blum & Th. Henning, 2000. Analogous experiments on the stickiness of micron-sized pre-planetary dust. Astrophys. J. 533, 454–471.

Rapp M., J. Hedin, I. Strelnikova, M. Friedrich, J Gumbel & F.-J. Lübken, 2005. Observations of positively charged nanoparticles in the night time polar mesosphere. Geophys. Res. Lett. 32(23), L23821.

Scoles, 1988. Giacinto: Atomic and molecular beam methods. New York, USA: Oxford University.

Thomas G.E., 1991. Mesospheric clouds and the physics of the mesopause region. Rev. Geophys. 29, 553–575.

Weitz D.A. & M. Oliveria, 1984. Fractal structures formed by kinetic aggregation of aqueous gold colloids. Phys. Rev. Lett. 52, 1433–1436.